Electrocatalysis (2019) 10:489–498
https://doi.org/10.1007/s12678-019-00531-8

ORIGINAL RESEARCH

Effects of Incorporated Iron or Cobalt on the Ethanol Oxidation Activity of Nickel (Oxy)Hydroxides in Alkaline Media

Daniel Martín-Yerga[1] · Gunnar Henriksson[2] · Ann Cornell[1]

Published online: 25 April 2019

Abstract

Nickel (oxy)hydroxides (NiO_xH_y) are promising cost-effective materials that exhibit a fair catalytic activity for the ethanol oxidation reaction (EOR) and could be used for sustainable energy conversion. Doping the NiO_xH_y structure with other metals could lead to enhanced catalytic properties but more research needs to be done to understand the role of the doping metal on the EOR. We prepared NiO_xH_y films doped with Fe or Co with different metallic ratios by electrodeposition and evaluated the EOR. We found a positive and negative effect on the catalytic activity after the incorporation of Co and Fe, respectively. Our results suggest that Ni atoms are the active sites for the EOR since Tafel slopes were similar on the binary and pristine nickel (oxy)hydroxides and that the formal potential of the Ni(II)/Ni(III) redox couple is a good descriptor for the EOR activity. This work also highlights the importance of controlled metal doping on catalysts and may help in the design and development of improved materials for the EOR.

Keywords Ethanol oxidation reaction · Nickel catalyst · Bimetallic catalysts · Electrocatalysis · Energy conversion

Introduction

In the last years, much effort has gone into the study of the electrochemical oxidation of alcohols for energy-related applications such as fuel cells [1] or hydrogen generation [2]. Ethanol is very appropriate due to its lower toxicity and higher energy density compared to methanol and to the possibility of renewable production from biomass [3]. Precious metal catalysts, especially Pt or Pd, show high electrocatalytic activity towards alcohol oxidation at low potentials. However, these materials have several drawbacks, such as limited global availability, high cost and deactivation issues by irreversible oxidation [4], or adsorption of poisoning species [5]. Therefore, the search for alternative earth-abundant electrocatalysts is still a constant concern. Nickel-based materials have been employed for the electrocatalytic ethanol oxidation [6–9] due to their low cost and high stability in alkaline media. Some strategies to enhance the overall catalytic activity for alcohol oxidation involve the exfoliation of the nickel layered hydroxide [6] in order to generate more reactive sites and expose a higher number of them to the solution, the synthesis of nanostructured materials with controlled shape [10, 11] or the use of effective catalyst supports such as carbon nanoflakes [12, 13] or nanofibers [14]. The incorporation of other metal atoms to the nickel (oxy)hydroxide (NiO_xH_y) structure is also a known method to change the catalytic properties of the material [15].

For instance, bimetallic Co/Ni materials have been reported for the ethanol oxidation reaction (EOR) [16–18]. Carbon nanofibers modified with NiCo alloyed nanoparticles showed increased catalytic activity for ethanol oxidation [16] compared to the same material formed only by nickel nanoparticles. These alloyed nanoparticles were synthesized at high temperatures in a reducing atmosphere leading to elemental NiCo, which needed electrochemical activation to generate active nickel hydroxides for ethanol oxidation. Interestingly, the oxidation activity was different for different metal ratios. Similar conclusions were reached using graphene as the

Electronic supplementary material The online version of this article (https://doi.org/10.1007/s12678-019-00531-8) contains supplementary material, which is available to authorized users.

✉ Daniel Martín-Yerga
dmy@kth.se

[1] Division of Applied Electrochemistry, Department of Chemical Engineering, KTH Royal Institute of Technology, Teknikringen 42, Floor 5, SE-100 44 Stockholm, Sweden

[2] Department of Fibre and Polymer Technology, KTH Royal Institute of Technology, SE-100 44 Stockholm, Sweden

carbon support for the CoNi alloyed nanoparticles [17]. Mixed Ni-Co oxides with different structural properties were also reported for the ethanol oxidation in alkaline media [18, 19]. For instance, carbon nanotubes-supported $NiCo_2O_4$ nanocomposite aerogels were used for this purpose [18]. The fibrous network of the nanotubes enabled the preparation of a material with uniform dispersion of $NiCo_2O4$ nanoparticles that showed excellent activity for ethanol oxidation. Materials with different geometric structures such as mesoporous $NiCo_2O_4$ fibers also showed enhanced activity compared to NiO and Co_3O_4 materials [19], demonstrating the positive synergistic effect of combining both materials.

Incorporation of Fe to NiO_xH_y has been widely employed for the oxygen evolution reaction (OER) as it has appeared as one of the best catalysts for this reaction [20], but just a few reports have been published using NiFe or Fe-based (oxy)hydroxides for alcohol oxidation. For instance, a multicomponent NiFe hydroxide nanocatalyst was evaluated for oxygen evolution and methanol oxidation [21]. A slightly enhanced response was found using the bimetallic NiFe catalyst compared to a Ni material, and the material only composed of Fe showed a very low activity for methanol oxidation. In contrast, FeOOH nanorods modified with fluorine atoms was demonstrated as a great catalyst for both OER and EOR [22]. In summary, as suggested by the different reported materials, there is enough evidence that nickel-based catalysts modified with other metal and non-metal atoms can enhance the EOR activity and it is a good strategy for designing improved materials. Thus, a systematic fundamental study of the incorporation of different metals to NiO_xH_y materials for the ethanol oxidation is needed to understand the role of metal doping, which would facilitate the design of new materials with enhanced properties.

In this work, we evaluate the effect of Fe or Co incorporation on the ethanol oxidation activity of electrodeposited NiO_xH_y films in alkaline solution. Metallic (oxy)hydroxide catalytic films with different metal ratios were prepared by a simple electrodeposition method. Analytical and electrochemical characterization of the catalysts was performed to gain a deeper understanding of the effect of metal doping on the nickel (oxy)hydroxides for the ethanol oxidation reaction. We conclude that the ethanol oxidation follows the same mechanism in the binary materials and the pristine nickel films, suggesting that only the nickel atoms are the active sites.

Material and Methods

Reagents and Solutions

$Ni(NO_3)_2$, $Co(NO_3)_2$, $FeCl_3$, $K_4[Fe(CN)_6]$, $NaNO_3$, ethanol absolute, and NaOH were purchased from Merck. For experiments in the absence of Fe, the NaOH electrolyte was cleaned to avoid impurities using $Ni(OH)_2$ as an Fe absorbent following a previously reported method [23]. Ultrapure water obtained with a Millipore DirectQ3 purification system from Millipore was used throughout this work.

Electrochemical Measurements

Electrochemical measurements were performed using a PAR273A potentiostat/galvanostat in a 100-mL glass three-electrode cell with a Pt mesh counter electrode and Ag/AgCl reference electrode (in contact with the solution through a Luggin capillary). A nickel disk (1 cm^2, geometric area) with electrodeposited films was employed as working electrode. A titanium disk electrode (1 cm^2, geometric area) was employed when the films were generated in the absence of nickel. The disks were polished before each experiment using 1-μm polishing alumina and washed with ultrapure water in an ultrasonic bath. The potential of the working electrode was converted in relation to the potential of the reversible hydrogen electrode (RHE) using the following Eq. 1:

$$E_{\text{vs.RHE}}\,(V) = E_{\text{vs.Ag/AgCl}} + 0.059\ \text{pH} + 0.197 \quad (1)$$

All the electrochemical experiments were performed at room temperature (21 ± 1 °C). After electrodeposition of catalysts, one cyclic voltammetry between + 0.8 V and 2.15 V (vs RHE) at 10 mV/s was performed in 0.1 M NaOH just before carrying out the ethanol oxidation experiments. Data shown in the figures is the average of three independent measurements and the error bars are the standard deviation of those measurements.

Electrochemical Deposition of Catalytic Materials

Electrodeposition was conducted onto disk electrodes using an unstirred solution with 0.1 M total metal concentration. When using Fe(III) solutions, sodium nitrate was added to keep a constant concentration of nitrate at 0.1 M in all the solutions. Electrochemical deposition was performed in a two-electrode cell with a carbon rod as a counterelectrode by applying a cathodic current of − 5 mA cm^{-2} for 30 s. After the deposition, the electrodes were rinsed with ultrapure water. In order to simplify the nomenclature, the binary materials are named as $Ni_{1-x}M_xO_yH_z$, where the x is the atomic fraction of the metals as recorded by energy-dispersive X-ray spectroscopy (vide infra).

Estimation of the Electrochemical Surface Area

Electrochemical surface area (ECSA) was estimated from the electrochemical double-layer capacitance (C_{dl}) of the catalytic

surface as widely employed in the literature [24–26]. Capacitance was determined by measuring the capacitive current associated with double-layer charging in a cyclic voltammetry experiment at different scan rates (10, 25, 50, 75, 100 mV s^{-1}). The potential range was from + 0.8 to + 0.9 V, where a non-Faradaic response was observed (Fig. S1). The capacitive current was measured at a potential of 0.85 V for the anodic and cathodic curves, and by plotting ($i = (i_{anodic} - i_{cathodic})/2$) versus the scan rate, the double-layer capacitance was estimated [27, 28]. Capacitive current is related to the double-layer capacitance and scan rate as given by Eq. 2. Figure S2 shows the linear relationships between the current and the scan rate obtained for different electrodeposited materials, which is consistent with capacitive charging behavior. The slope of this representation provides the C_{dl}. Then, the ECSA of the catalyst was calculated from the C_{dl} using Eq. 3 and the specific capacitance (C_s) of the material. For metallic oxides/hydroxides, the specific capacitances are usually near 0.04 mF cm^{-2} in alkaline media [25] and this value was used for the calculations. Figure S3 shows the ECSA calculated using this method for the different electrodes prepared by catalyst electrodeposition. Current densities for the voltammetric data were normalized by the ECSA hereinafter.

$$i_c = C_{dl} v \tag{2}$$

$$\mathrm{ECSA} = \frac{C_{dl}}{C_s} \tag{3}$$

Compositional and Structural Characterization of Catalysts

The catalysts were electrodeposited as previously described and to avoid the effect of the electrode substrate in the characterization, the films were rinsed with ultrapure water, left to dry, and scraped carefully to get a powdered sample. This process was repeated several times in order to get enough material for the characterization. The compositional analysis and determination of the experimental metallic ratio of the catalyst films were carried out by energy-dispersive X-ray spectroscopy (EDS). The powdered samples were placed on carbon conductive tabs and analyzed on a JEOL JSM-7000F scanning electron microscope using the integrated EDS detector. An acceleration voltage of 15 kV was applied. The crystalline properties of the catalysts were analyzed using powder X-ray diffraction (XRD) recorded with a PANalytical PRO MPD diffractometer in Bragg-Brentano geometry with 1.5406 Å Cu Kα1 radiation, using a 2θ range of 8.0–70.0° and a step size of 0.033°. Samples for XRD analysis were carefully grinded to a homogenous powder and deposited with the aid of isopropanol on a zero-background sample holder based on a Si wafer for use in reflection geometry.

Results and Discussion

Analytical Characterization of Metallic Catalysts

Catalysts were characterized by EDS to obtain information about the chemical composition. Figure 1a shows the EDS spectrum of the catalyst formed by electrodeposition from a monometallic nickel solution. The spectrum shows the presence of nickel and also a significant presence of oxygen, which suggests that the material is formed by some kind of nickel oxide or hydroxide. A signal for carbon was also observed in the spectra, coming from the carbon tab used to hold the powdered sample. Similar results were found for the catalysts formed by the other monometallic precursors (Fe or Co) as can be observed in Fig. 1b and c . These spectra only showed the presence of the precursor metal and oxygen. Spectra for bimetallic materials (Fig. S4) showed the presence of both metals, and the experimental atomic metallic ratio was estimated (Table 1). In general, the catalysts had experimental compositions with lower Ni:M ratios than the precursor solution.

XRD analysis of selected samples was performed in order to determine the crystallographic features of the catalytic materials. In general, a low crystallinity was found for all the analyzed nickel-based materials. Figure 2 (blue line) shows the XRD pattern of the monometallic nickel catalyst. Several wide peaks are observed at 2Θ values of 11.3, 19.3, 33.3, 38.6, and 59.7°, which can be ascribed to the (001), (100), (110), (200), and (301) lattice planes of an α-$Ni(OH)_2$ phase [29], also in agreement with the low crystalline pattern [23, 30, 31] due to the quite disordered structure. The generation of α-$Ni(OH)_2$ can be explained since this phase can be formed when a rapid precipitation process occurs from Ni^{2+} in presence of OH^- [32], which is a kinetically driven process. Therefore, we propose that the main mechanism of the precipitation comes by reduction of NO_3^- ions [32] or hydrogen evolution that generates a local environment near the electrode surface with a high concentration of OH^- (Eqs. 4–6) leading to deposition of disordered α-$Ni(OH)_2$. It is well known that conversion of α-$Ni(OH)_2$ to β-$Ni(OH)_2$ is possible by repeated cycling the electrode surface in alkaline media or thermal treatment since it is the most thermodynamically stable phase. However, it has also been demonstrated that α-$Ni(OH)_2$ is more catalytically active than β-$Ni(OH)_2$ for alcohol or water oxidation and that the oxidation to Ni(III) occurs at less positive potentials [32]. Enhanced electrocatalysis of α-$Ni(OH)_2$ can also be explained by other factors such as the more facile ion-solvent intercalation [32] or the formation of a γ-NiOOH

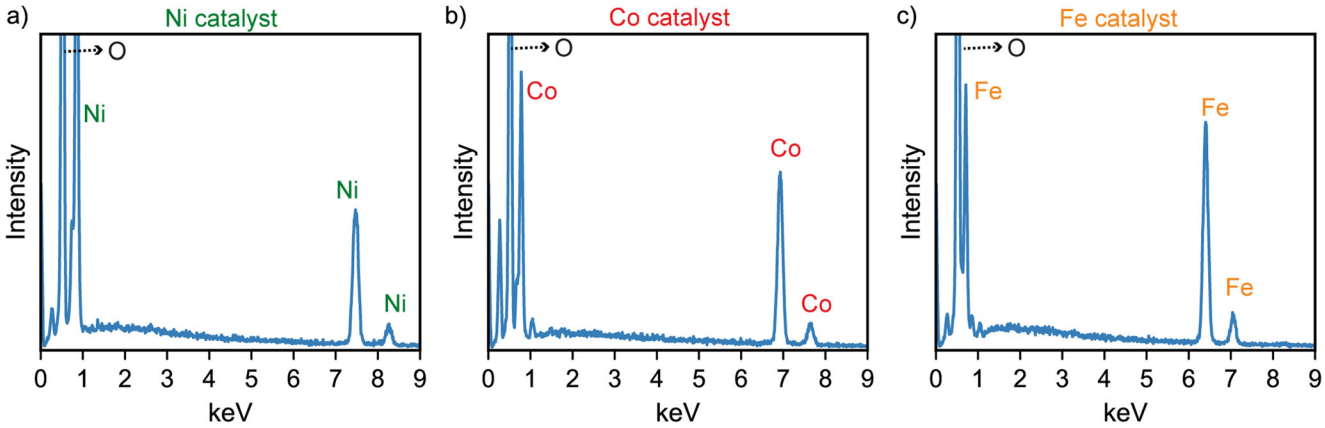

Fig. 1 Spectra obtained by energy-dispersive X-ray spectroscopy of the catalytic materials using monometallic precursor solutions: **a** nickel catalyst, **b** cobalt catalyst, **c** iron catalyst. The different metals composing the catalysts can be clearly differentiated by using the K lines from the spectra

phase which has a higher oxidation state than β-NiOOH [33, 34], and, consequently, higher oxidizing power.

$$NO_3^- + 7H_2O + 8\,e^- \rightarrow NH_4^+ + 10\,OH^- \quad (4)$$

$$2\,H_2O + 2e^- \rightarrow\ H_2 + 2\,OH^- \quad (5)$$

$$Ni^{2+} + 2\,OH^- \rightarrow Ni(OH)_2 \quad (6)$$

Figure 2 (red line) also shows the XRD pattern of the monometallic cobalt material, CoO_xH_y. In this case, some wide peaks were observed at 2Θ of 10.8, 33.7, and 51.5, and around 60°, and narrower peaks, suggesting a more crystalline phase, were also observed at 2Θ of 19.1 and 38.0°. It may be challenging to assign some of these peaks to the correct structure, but it seems clear that the wide peak at 10.8° can be assigned to the (001) lattice plane of low-crystalline α-$Co(OH)_2$ [35] while the narrow peak at 19.1° can be definitely ascribed to the (001) lattice plane of crystalline β-$Co(OH)_2$ [36]. Therefore, this material seems to be a combination of the α and β phases of $Co(OH)_2$. XRD patterns for the bimetallic materials ($Ni_{0.69}Co_{0.31}O_xH_y$ and $Ni_{0.77}Fe_{0.23}O_xH_y$) only showed similar features to those observed for α-$Ni(OH)_2$ with a general small shift of the XRD peaks. This suggests the successful incorporation of Co or Fe leading to a more disordered α-$Ni(OH)_2$ structure.

Table 1 Experimental metal ratio for the different catalysts obtained by EDS data compared to the initial metal ratio of the precursor solution

Precursor solution (Ni:M)	EDS data (Ni:Co)	EDS data (Ni:Fe)
99:1	–	99:1
95:5	–	89:11
90:10	86:14	77:23
80:20	69:31	63:37
60:40	51:49	40:60

Effects of Incorporated Metals on the Ethanol Oxidation

Cyclic voltammograms at a scan rate of 10 mV s^{-1} were recorded in 0.1 M NaOH to study the redox processes of the nickel-electrodeposited films. The typical redox processes for the oxidation and reduction of Ni(II)/Ni(III) species in alkaline media were observed in the voltammograms (Fig. 3a, blue curve) with anodic and cathodic peak potentials of 1.48 and 1.28 V (vs RHE), respectively. These redox waves are typically attributed to the anodic oxidation of $Ni(OH)_2$ to the oxyhydroxide species, NiOOH, and the cathodic reduction back to the initial species (Eq. 7). However, it has also been proposed that the reaction entails the transfer of more than 1 e^- per Ni atom and higher oxidation states than + 3 could also be formed [34, 37, 38]. This may be related to the formation of

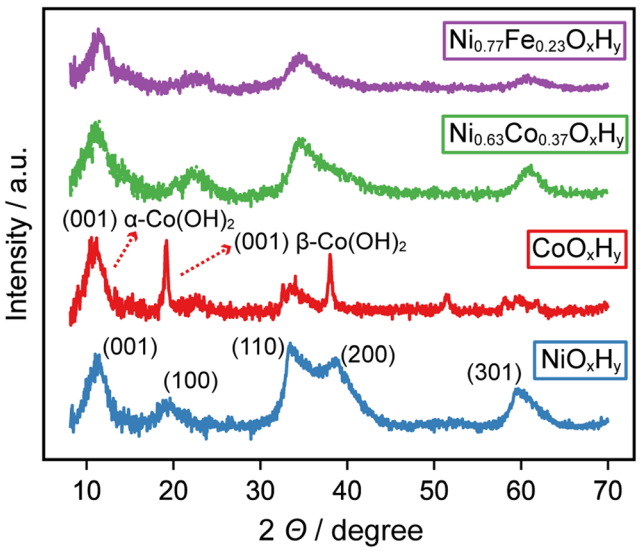

Fig. 2 X-ray diffraction patterns for selected electrodeposited catalysts: NiO_xH_y (blue line), CoO_xH_y (red line), $Ni_{0.63}Co_{0.37}O_xH_y$ (green line), and $Ni_{0.77}Fe_{0.23}O_xH_y$ (purple line)

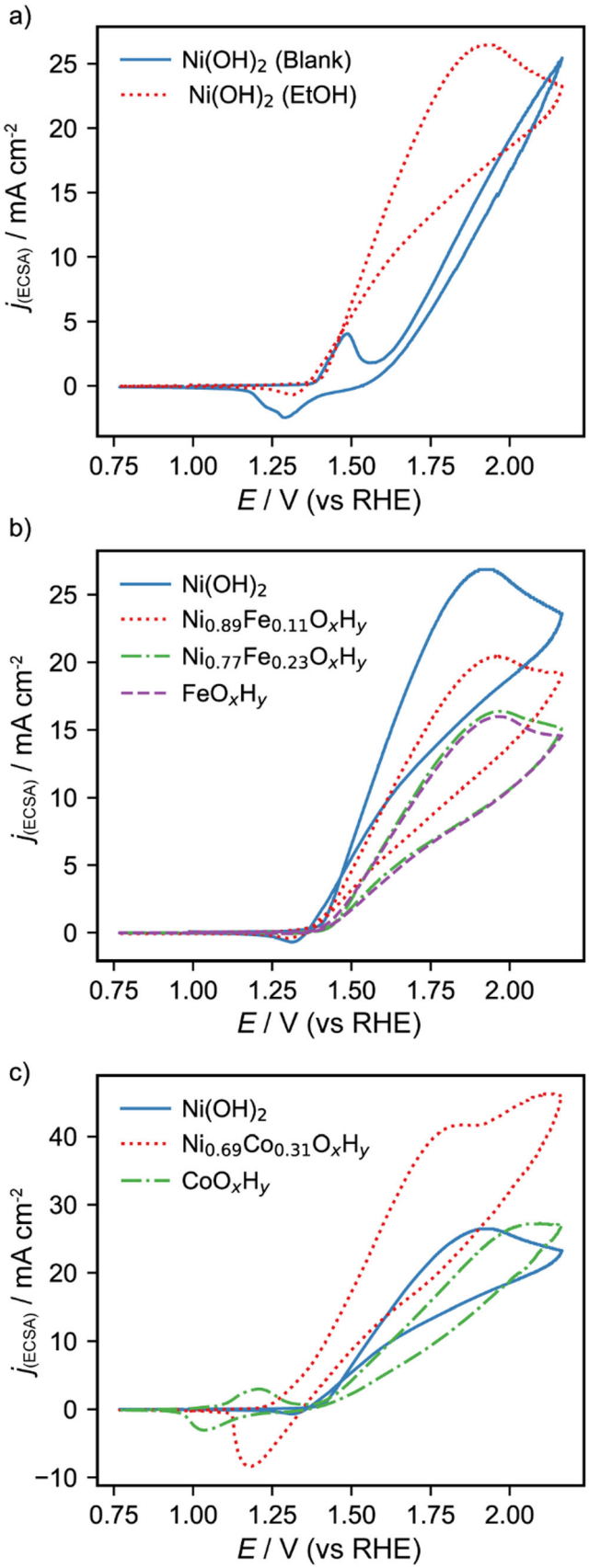

◀ **Fig. 3** **a** Voltammograms obtained for the electrodeposited $Ni(OH)_2$ films in the absence (blue solid curve) and presence (red dotted curve) of 1 M ethanol in 0.1 M NaOH. **b** Voltammograms for 1 M ethanol in 0.1 M NaOH using electrodes modified with $Ni(OH)_2$ (blue solid curve), $Ni_{0.89}Fe_{0.11}O_xH_y$ (red dotted curve), $Ni_{0.77}Fe_{0.23}O_xH_y$ (green dashed curve), and FeO_xH_y (purple dashed curve). **c** Voltammograms for 1 M ethanol in 0.1 M NaOH using electrodes modified with $Ni(OH)_2$ (blue solid curve), $Ni_{0.69}Co_{0.31}O_xH_y$ (red dotted curve), and CoO_xH_y (green dashed curve). Scan rate was 10 mV s^{-1} in all cases

different phases of NiOOH. For instance, oxidation of α-$Ni(OH)_2$ is assumed to generate γ-NiOOH [33], which has a higher formal oxidation state (between + 3.5–3.67) [34, 38] than β-NiOOH typically generated from β-$Ni(OH)_2$. This usually results in enhanced catalytic activity for both alcohol [32] and water [31] oxidation. Another anodic process can be observed in the voltammetric curve of the blank solution at higher potentials than the NiOOH formation, which is assigned to the OER.

$$Ni(OH)_2 + OH^- \rightleftarrows NiOOH + H_2O + e^- \quad (7)$$

In the presence of 1 M ethanol (Fig. 3a, red curve), a strong increment of the anodic current was observed with a peak potential at about 1.91 V (vs RHE), which is assigned to the EOR. Fleischmann et al. [39] proposed that the Ni(III) is directly involved in the alcohol oxidation and it has been supported by other works [40, 41]. This mechanism has been disputed because in some cases, the oxidation proceeds at higher potentials than the formation of Ni(III) [42, 43], which questions the direct involvement of the Ni(III) sites. Our results are in good agreement with the former possibility as the onset potential of the EOR coincides with the potential of the Ni(II) oxidation, suggesting that the Ni(III) formed in this process is strongly involved in the EOR. A mechanism of the EOR by NiOOH has been previously proposed (Eq. 8) [40], and widely studied under different conditions [44–47]. Briefly, in this mechanism, the electrogenerated Ni(III) can oxidize ethanol by an initial dehydrogenation step typically leading to acetaldehyde and/or acetate [48]. The lower cathodic peak current of the Ni(III) reduction in presence of ethanol is also a strong indication of the direct involvement of Ni(III) in the EOR (Ni(III) is reduced during ethanol oxidation and less is available for the electrochemical reduction).

$$NiOOH + CH_3CH_2OH \longrightarrow Ni(OH)_2 + \text{oxidation products} \quad (8)$$

The voltammograms obtained for the bare Ni electrode are also shown in Fig. S5 for comparison. For the bare electrode, a significantly lower activity for the EOR is observed. This fact demonstrates that the electrodeposited nickel film is essential to achieve a high catalytic activity for the EOR.

The effect of incorporating Fe or Co into the NiO_xH_y films was studied. The electrodeposition was performed under the

same conditions but varying the ratio Ni:M and thereby the concentrations of the incorporated metal. Figure 3b shows representative voltammetric responses for the EOR using the $Ni(OH)_2$, $Ni_{0.89}Fe_{0.11}O_xH_y$, $Ni_{0.77}Fe_{0.23}O_xH_y$, and FeO_xH_y films. As observed, the incorporation of Fe decreased the catalytic activity leading to higher onset potentials compared to the pristine Ni films while the peak current densities were also decreased. Figure 3c shows the voltammetric response for the EOR using the $Ni(OH)_2$, $Ni_{0.69}Co_{0.31}O_xH_y$, and CoO_xH_y films. An enhanced catalytic activity is observed for the binary NiCo catalysts compared to the $Ni(OH)_2$ catalyst, suggesting a positive effect of the Co incorporation. Previous results with DFT calculations have shown that the Co atoms in binary NiCo materials could improve the adsorption of alcohols on the catalytic sites and decrease the poisoning of the surface resulting in enhanced catalytic activity [49]. It is reasonable to assume a similar behavior for the EOR in these bimetallic catalysts. Interestingly, for the mixed NiCo catalysts, two different oxidation processes were observed in the same voltammetric curve (Fig. 3c, red dotted curve): one dominating at lower potentials (peak potential at 1.79 V vs RHE) and the other one dominating at higher potentials (peak potential at 2.07 V vs RHE). The peak potential in the latter case is close to that observed for the CoO_xH_y catalyst, suggesting that two different types of active sites are available. Another possibility is that the ethanol reaction pathway would result in an initial subproduct able to be oxidized at a slightly higher potential than ethanol. Low catalytic activity was observed for the CoO_xH_y catalyst in agreement with previous results [50], with higher onset potentials than for $Ni(OH)_2$. The EOR using the CoO_xH_y catalyst occurred at potentials higher than the oxidation of Co(II), suggesting a different mechanism than for Ni-based materials. Figure 4 shows some of the voltammograms obtained in the absence of ethanol using different electrodeposited materials. In general, the incorporation of Fe to the Ni catalyst shifted the peak potential of the Ni(II) oxidation towards more positive potentials, while Co incorporation had the opposite effect. This fact agrees with the activity observed for the EOR and also suggests that the formed NiOOH plays a direct role in the ethanol oxidation using Ni-based materials.

Effects of the Metallic Ratio on the Catalytic Activity and Reaction Mechanism

The effect of the ratio of incorporated metal on the EOR catalytic activity was evaluated by following the potential at a current density of 10 mA cm^{-2}. Figure 5 shows the variation of this potential in relation to the percentage of the incorporated Co or Fe into the NiO_xH_y and in the absence of Ni (FeO_xH_y or CoO_xH_y). Incorporation of Fe affected the catalytic activity negatively, increasing the potential at 10 mA cm^{-2}. Catalysts formed by NiFe (oxy)hydroxides are one of the top catalysts for the OER and it has been proposed that Fe atoms are the active sites for that reaction [37, 51]. The results found for the EOR suggest that these reactions are affected by different factors. In contrast, the incorporation of Co positively affected the catalytic activity for the EOR decreasing the potential necessary to achieve the same current density. The optimal catalyst was $Ni_{0.69}Co_{0.31}O_xH_y$, which showed the highest activity (in terms of onset potential and peak current density). When CoO_xH_y was employed as the catalyst material, the potential increased up to values similar to those found for the Fe-based catalysts, indicating a lower activity than for NiCo or pristine Ni films. In summary, our results suggest that the incorporation of different cations to the Ni (oxy)hydroxide structure can influence the catalytic

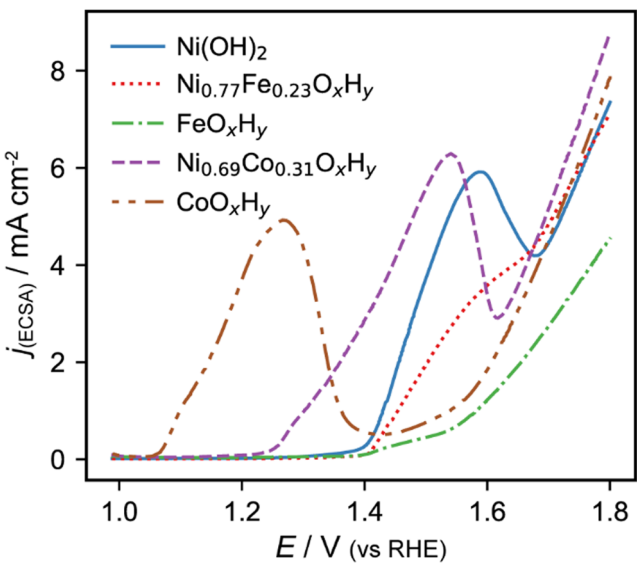

Fig. 4 Anodic part of the voltammograms obtained in 0.1 M NaOH using different electrodeposited materials. Scan rate was 10 mV s^{-1}

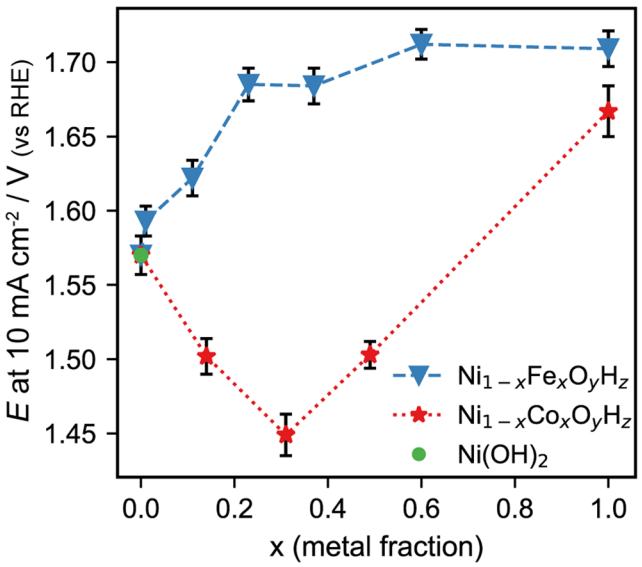

Fig. 5 Potential at 10 mA cm^{-2} for the EOR with different $Ni_{1-x}M_xO_yH_z$ catalysts in relation to the content of the doping metal

activity in different ways. It is worth to mention that the synthesis of Ni-based materials employed for the EOR should consider the possibility of accidentally incorporating metallic impurities that could influence the catalytic activity of the material as shown for Fe in OER catalysts [23].

In order to evaluate the effect of the metal incorporation on the reaction mechanism, an analysis of Tafel slopes was performed. In this case, the voltammograms were recorded at 2 mV s^{-1} in order to mimic a steady-state behavior and the EOR was evaluated at potentials close to the onset potential. The Tafel slopes obtained by plotting the potential versus the logarithm of the current density provides information associated with the rate determining steps of the electrochemical reaction. Figure 6 shows the effect of different incorporated metals on the Tafel slope. A similar value (60–70 mV dec^{-1}) was found for the Ni-based catalysts with incorporated Fe or Co. The observation of similar Tafel slopes for all the Ni-based catalysts suggest a similar reaction mechanism with a similar rate-determining step for the EOR. The Tafel slopes obtained for the FeO_xH_y and CoO_xH_y materials were significantly higher, indicating more sluggish kinetics or a different reaction mechanism. These results are in agreement with Ni alone being the active sites involved directly in the EOR because the incorporation of Fe or Co changes the catalytic activity (increased by Co, decreased by Fe) as observed in the voltammetric curves (onset potentials, current densities) but does not show any significant variation on the reaction mechanism or kinetics as suggested by the observed similar Tafel slopes. It is also interesting to compare the Tafel slopes obtained for the nickel-based catalysts in our work with other previously reported values. Many previous works using nickel-based catalysts [52–54] have reported higher Tafel slopes, ranging from 120 to 160 mV dec^{-1} in most cases. However, the catalyst materials were usually synthesized by thermal processes at high temperatures or pretreated by electrochemical cycling, which usually leads to the formation of the more thermodynamically favorable and crystalline structure, β-$Ni(OH)_2$. It is well known that α-$Ni(OH)_2$ can form γ-NiOOH during oxidation, which shows a significantly higher catalytic activity for alcohol oxidation than the β-$Ni(OH)_2$/β-NiOOH system [32]. Therefore, it is reasonable to assume that the enhanced catalytic activity of the α-$Ni(OH)_2$/γ-NiOOH system could lead to a lower Tafel slope. Low slopes, similar to our results, were found in the initial works by Fleischmann et al. using nickel electrodes for organic compounds oxidation [39, 55] when they proposed the oxidation mechanism involving Ni(III). Similar or even lower Tafel slope values for ethanol oxidation have been found at optimized multimaterial noble-metal catalysts [56, 57].

Effect of the Electronic Properties of Nickel Atoms on the Activity

It has been previously proposed that the addition of different metals to the structure of NiO_xH_y could increase the catalytic activity of these materials towards the OER by an electron-withdrawing effect from the nickel sites to the incorporated atoms [23, 58, 59]. The formal potential $E^{0\prime}$ of the nickel redox couple ($Ni^{2+/3+}$) could then be an activity descriptor if these atoms are involved in the reaction (active sites) and if the electronic properties of the nickel atoms affect the catalytic activity. Figure 7 shows the correlation between the $E^{0\prime}$ of the nickel redox couple for different metallic ratios and the potential at 10 mA cm^{-2}. The $E^{0\prime}$ was calculated as the average of the anodic and cathodic peak potentials of the Ni(II)/Ni(III) processes in the absence of ethanol. The incorporation

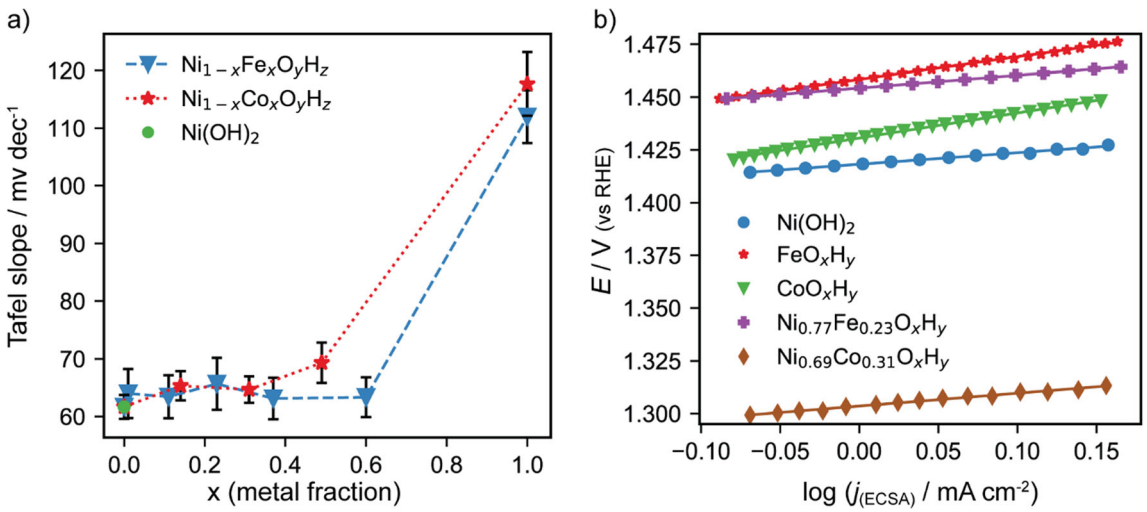

Fig. 6 **a** Tafel slopes for the EOR with the different $Ni_{1-x}M_xO_yH_z$ catalysts in relation to the content of the doping metal. **b** Voltammetric data to calculate the Tafel slopes for specific $Ni_{1-x}M_xO_yH_z$ catalysts in 1 M ethanol and 0.1 M NaOH at a scan rate of 2 mV s^{-1}

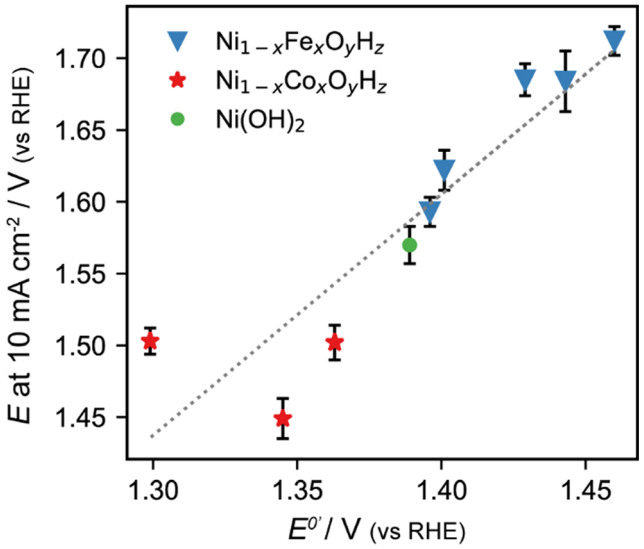

Fig. 7 Potential at 10 mA cm^{-2} for the EOR with the different $Ni_{1-x}M_xO_yH_z$ catalysts in relation to the formal potential of the Ni(II)/Ni(III) redox processes

of Fe increased the $E^{0\prime}$ while Co decreased it compared to pristine Ni. There seems to be a correlation between the values of $E^{0\prime}$ and the catalytic activity (for different metallic ratios), so that high values of the nickel $E^{0\prime}$ have a negative influence on the catalytic activity and lower values enhance the catalytic activity. These results suggest that the electronic properties of the nickel atoms, as reported by the formal potential of the Ni redox couple, affect the ethanol oxidation. Adding Fe makes it more difficult to oxidize Ni(II), and the opposite happens with Co, which could be the reason why the overpotential for the NiCo catalysts is lower. These facts would agree with the direct involvement of Ni(III) in the EOR and with Ni being the active site in these catalysts. It is worth to mention that the catalytic activity and/or Ni(II) oxidation of bimetallic materials may also be influenced by other processes such as the adsorption energies of the reactants/products or parameters influencing the diffusion processes within the (oxy)hydroxide structure such as the crystal lattice constant, presence of counterions [60], availability of vacant sites [61], or local stress field [62]. The combined effect of those properties would probably explain the different activity of the catalyst at different metallic ratios. In any case, our results suggest that the electronic properties of the nickel active sites may play an important role during the ethanol oxidation. Thus, the formal potential of the Ni(II)/Ni(III) redox couple seems to be a good general descriptor of EOR activity on nickel bimetallic catalysts, and its calculation could be a simple and rapid method to understand the activity of different nickel-based catalysts. In this regard, it may be very interesting to evaluate materials formed by incorporation of Y to nickel hydroxides, since they seem to shift the formal potential to less positive values [63].

Conclusions

We evaluated Ni (oxy)hydroxide films with the incorporation of increasing amounts of Fe or Co for the EOR. Co doping led to enhanced EOR catalysis while Fe addition showed a negative effect. A Tafel slope analysis indicated that the EOR follows the same mechanism in pristine nickel hydroxide than in binary catalysts. The catalytic activity was well correlated with the electronic properties of the nickel atoms as given by the formal potential of the Ni(II)/Ni(III) redox couple. Both findings are consistent with the nickel atoms being the active sites for the EOR. These results help to understand the effects of metallic doping in nickel (oxy)hydroxides on the catalytic activity and mechanism for the EOR and may be significant for the development of improved materials.

Funding information The authors are grateful for the support from the Swedish Energy Agency (Ref. 2017-004908).

References

1. M.C. Figueiredo, A. Santasalo-Aarnio, F.J. Vidal-Iglesias, J. Solla-Gullón, J.M. Feliu, K. Kontturi, T. Kallio, Tailoring properties of platinum supported catalysts by irreversible adsorbed adatoms toward ethanol oxidation for direct ethanol fuel cells. Appl. Catal. B Environ. **140–141**, 378–385 (2013)
2. S. Tuomi, A. Santasalo-Aarnio, P. Kanninen, T. Kallio, Hydrogen production by methanol–water solution electrolysis with an alkaline membrane cell. J. Power Sources **229**, 32–35 (2013)
3. S. Bastianoni, N. Marchettini, Ethanol production from biomass: analysis of process efficiency and sustainability. Biomass Bioenergy **11**(5), 411–418 (1996)
4. L. Wang, A. Lavacchi, M. Bellini, F. D'Acapito, F. Di Benedetto, M. Innocenti, H. A. Miller, G. Montegrossi, C. Zafferoni, and F. Vizza, Deactivation of palladium electrocatalysts for alcohols oxidation in basic electrolytes. Electrochim. Acta **177**, 100-106 (2015)
5. J. Liu, F.R. Lucci, M. Yang, S. Lee, M.D. Marcinkowski, A.J. Therrien, C.T. Williams, E.C.H. Sykes, M. Flytzani-Stephanopoulos, Tackling CO poisoning with single-atom alloy catalysts. J. Am. Chem. Soc. **138**(20), 6396–6399 (2016)
6. L. Xu, Z. Wang, X. Chen, Z. Qu, F. Li, W. Yang, Ultrathin layered double hydroxide nanosheets with Ni(III) active species obtained by exfoliation for highly efficient ethanol electrooxidation. Electrochim. Acta **260**, 898–904 (2018)
7. A.B. Soliman, H.S. Abdel-Samad, S.S. Abdel Rehim, M.A. Ahmed, H.H. Hassan, High performance nano-Ni/graphite electrode for electro-oxidation in direct alkaline ethanol fuel cells. J. Power Sources **325**, 653–663 (2016)
8. I. Danaee, M. Jafarian, M. Sharafi, F. Gobal, A kinetic investigation of ethanol oxidation on a nickel oxyhydroxide electrode. J. Electrochem. Sci. Technol. **3**(1), 50–56 (2012)
9. H. Wang, Y. Cao, J. Li, J. Yu, H. Gao, Y. Zhao, Y.-U. Kwon, G. Li, Preparation of Ni/NiO-C catalyst with NiO crystal: catalytic

performance and mechanism for ethanol oxidation in alkaline solution. Ionics (Kiel). **24**(9), 2745–2752 (2018)
10. F. Muench, M. Oezaslan, M. Rauber, S. Kaserer, A. Fuchs, E. Mankel, J. Brötz, P. Strasser, C. Roth, W. Ensinger, Electroless synthesis of nanostructured nickel and nickel–boron tubes and their performance as unsupported ethanol electrooxidation catalysts. J. Power Sources **222**, 243–252 (2013)
11. W. Shi, H. Gao, J. Yu, M. Jia, T. Dai, Y. Zhao, J. Xu, G. Li, One-step synthesis of N-doped activated carbon with controllable Ni nanorods for ethanol oxidation. Electrochim. Acta **220**, 486–492 (2016)
12. A. Ahmadi Daryakenari, D. Hosseini, Y. L. Ho, T. Saito, A. Apostoluk, C. R. Müller, and J. J. Delaunay, Single-step electrophoretic deposition of non-noble metal catalyst layer with low onset voltage for ethanol electro-oxidation. ACS Appl. Mater. Interfaces 8, 15975 (2016), 25, 15984
13. A.A. Daryakenari, D. Hosseini, M.H. Mirfasih, A. Apostoluk, C.R. Müller, J.-J. Delaunay, Formation of NiO nanoparticle-attached nanographitic flake layers deposited by pulsed electrophoretic deposition for ethanol electro-oxidation. J. Alloys Compd. **698**, 571–576 (2017)
14. N.A.M. Barakat, H.M. Moustafa, M.M. Nassar, M.A. Abdelkareem, M.S. Mahmoud, A.A. Almajid, K.A. Khalil, Distinct influence for carbon nano-morphology on the activity and optimum metal loading of Ni/C composite used for ethanol oxidation. Electrochim. Acta **182**, 143–155 (2015)
15. M.S. Burke, L.J. Enman, A.S. Batchellor, S. Zou, S.W. Boettcher, Oxygen evolution reaction electrocatalysis on transition metal oxides and (oxy)hydroxides: activity trends and design principles. Chem. Mater. **27**(22), 7549–7558 (2015)
16. N.A.M. Barakat, M. Motlak, A.A. Elzatahry, K.A. Khalil, E.A.M. Abdelghani, Ni_xCo_{1-x} alloy nanoparticle-doped carbon nanofibers as effective non-precious catalyst for ethanol oxidation. Int. J. Hydrog. Energy **39**(1), 305–316 (2014)
17. N.A.M. Barakat, M. Motlak, B.H. Lim, M.H. El-Newehy, S.S. Al-Deyab, Effective and stable CoNi alloy-loaded graphene for ethanol oxidation in alkaline medium. J. Electrochem. Soc. **161**(12), F1194–F1201 (2014)
18. S. S. Jayaseelan, T. Ko, S. Radhakrishnan, C. Yang, H.-Y. Kim, and B. Kim, Novel MWCNT interconnected $NiCo_2O_4$ aerogels prepared by a supercritical CO_2 drying method for ethanol electrooxidation in alkaline media. Int. J. Hydrog. Energy **41**(31), 13504-13512 (2016)
19. J. Zhan, M. Cai, C. Zhang, C. Wang, Synthesis of mesoporous $NiCo_2O_4$ fibers and their electrocatalytic activity on direct oxidation of ethanol in alkaline media. Electrochim. Acta **154**, 70–76 (2015)
20. M.S. Burke, S. Zou, L.J. Enman, J.E. Kellon, C.A. Gabor, E. Pledger, S.W. Boettcher, Revised oxygen evolution reaction activity trends for first-row transition-metal (oxy)hydroxides in alkaline media. J. Phys. Chem. Lett. **6**(18), 3737–3742 (2015)
21. S.L. Candelaria, N.M. Bedford, T.J. Woehl, N.S. Rentz, A.R. Showalter, S. Pylypenko, B.A. Bunker, S. Lee, B. Reinhart, Y. Ren, S.P. Ertem, E.B. Coughlin, N.A. Sather, J.L. Horan, A.M. Herring, L.F. Greenlee, Multi-component Fe–Ni hydroxide nanocatalyst for oxygen evolution and methanol oxidation reactions under alkaline conditions. ACS Catal. **7**(1), 365–379 (2017)
22. G.-F. Chen, Y. Luo, L.-X. Ding, H. Wang, Low-voltage electrolytic hydrogen production derived from efficient water and ethanol oxidation on fluorine-modified FeOOH anode. ACS Catal. **8**(1), 526–530 (2018)
23. L. Trotochaud, S.L. Young, J.K. Ranney, S.W. Boettcher, Nickel–iron oxyhydroxide oxygen-evolution electrocatalysts: the role of intentional and incidental iron incorporation. J. Am. Chem. Soc. **136**(18), 6744–6753 (2014)
24. S. Trasatti, O.A. Petrii, Real surface area measurements in electrochemistry. J. Electroanal. Chem. **327**(1-2), 353–376 (1992)
25. C. C. L. McCrory, S. Jung, J. C. Peters, and T. F. Jaramillo, Benchmarking heterogeneous electrocatalysts for the oxygen evolution reaction. J. Am. Chem. Soc. **135**(45), 16977-16987 (2013)
26. O. Diaz-Morales, I. Ledezma-Yanez, M.T.M. Koper, F. Calle-Vallejo, Guidelines for the rational design of Ni-based double hydroxide electrocatalysts for the oxygen evolution reaction. ACS Catal. **5**(9), 5380–5387 (2015)
27. K. Fan, H. Chen, Y. Ji, H. Huang, P.M. Claesson, Q. Daniel, B. Philippe, H. Rensmo, F. Li, Y. Luo, L. Sun, Nickel–vanadium monolayer double hydroxide for efficient electrochemical water oxidation. Nat. Commun. **7**(1), 11981 (2016)
28. K. Fan, Y. Ji, H. Zou, J. Zhang, B. Zhu, H. Chen, Q. Daniel, Y. Luo, J. Yu, L. Sun, Hollow iron-vanadium composite spheres: A highly efficient iron-based water oxidation electrocatalyst without the need for nickel or cobalt. Angew. Chem. Int. Ed. **56**(12), 3289–3293 (2017)
29. D.S. Hall, D.J. Lockwood, C. Bock, B.R. MacDougall, Nickel hydroxides and related materials: a review of their structures, synthesis and properties. Proc. R. Soc. A Math. Phys. Eng. Sci. **471**(2174), 20140792 (2014)
30. M.-S. Kim, A study of the electrochemical redox behavior of electrochemically precipitated nickel hydroxides using electrochemical quartz crystal microbalance. J. Electrochem. Soc. **144**(5), 1537 (1997)
31. M. Gao, W. Sheng, Z. Zhuang, Q. Fang, S. Gu, J. Jiang, Y. Yan, Efficient water oxidation using nanostructured α-nickel-hydroxide as an electrocatalyst. J. Am. Chem. Soc. **136**(19), 7077–7084 (2014)
32. S. P. E, D. Liu, R. A. Lazenby, J. Sloan, M. Vidotti, P. R. Unwin, and J. V. Macpherson, Electrodeposition of nickel hydroxide nanoparticles on carbon nanotube electrodes: correlation of particle crystallography with electrocatalytic properties. J. Phys. Chem. C **120**(29), 16059-16068 (2016)
33. B.C. Cornilsen, X. Shan, P.L. Loyselle, Structural comparison of nickel electrodes and precursor phases. J. Power Sources **29**(3-4), 453–466 (1990)
34. P.V. Kamath, M. Dixit, L. Indira, A.K. Shukla, V.G. Kumar, N. Munichandraiah, Stabilized α-$Ni(OH)_2$ as electrode material for alkaline secondary cells. J. Electrochem. Soc. **141**(11), 2956 (1994)
35. Y. Xu, Z. Liu, D. Chen, Y. Song, R. Wang, Synthesis and electrochemical properties of porous α-$Co(OH)_2$ and Co_3O_4 microspheres. Prog. Nat. Sci. Mater. Int. **27**(2), 197–202 (2017)
36. L. Wang, J. Fu, Y. Zhang, X. Liu, Y. Yin, L. Dong, S. Chen, Mesoporous β-$Co(OH)_2$ nanowafers and nanohexagonals obtained synchronously in one solution and their electrochemical hydrogen storage properties. Prog. Nat. Sci. Mater. Int. **26**(6), 555–561 (2016)
37. M. B. Stevens, C. D. M. Trang, L. J. Enman, J. Deng, and S. W. Boettcher, Reactive Fe-sites in Ni/Fe (oxy)hydroxide are responsible for exceptional oxygen electrocatalysis activity. J. Am. Chem. Soc. 139, 11361 (2017), 33, 11364
38. M.E.G. Lyons, M.P. Brandon, A comparative study of the oxygen evolution reaction on oxidised nickel, cobalt and iron electrodes in base. J. Electroanal. Chem. **641**(1-2), 119–130 (2010)
39. M. Fleischmann, K. Korinek, D. Pletcher, The oxidation of organic compounds at a nickel anode in alkaline solution. J. Electroanal. Chem. Interfacial Electrochem. **31**(1), 39–49 (1971)
40. H.B. Hassan, Z.A. Hamid, Electrodeposited Ni–Cr_2O_3 nanocomposite anodes for ethanol electrooxidation. Int. J. Hydrog. Energy **36**(8), 5117–5127 (2011)
41. F. Gobal, Y. Valadbeigi, L.M. Kasmaee, On the significance of hydroxide ion in the electro-oxidation of methanol on Ni. J. Electroanal. Chem. **650**(2), 219–225 (2011)
42. G. Vértes, G. Horányi, Some problems of the kinetics of the oxidation of organic compounds at oxide-covered nickel electrodes. J. Electroanal. Chem. Interfacial Electrochem. **52**(1), 47–53 (1974)

43. J. Taraszewska, G. Rosłonek, Electrocatalytic oxidation of methanol on a glassy carbon electrode modified by nickel hydroxide formed by ex situ chemical precipitation. J. Electroanal. Chem. **364**(1-2), 209–213 (1994)
44. A.F.B. Barbosa, V.L. Oliveira, J. van Drunen, G. Tremiliosi-Filho, Ethanol electro-oxidation reaction using a polycrystalline nickel electrode in alkaline media: temperature influence and reaction mechanism. J. Electroanal. Chem. **746**, 31–38 (2015)
45. A.J. Motheo, S.A.S. Machado, F.J.B. Rabelo, J.R. Santos Jr, Electrochemical study of ethanol oxidation on nickel in alkaline media. J. Braz. Chem. Soc. **5**(3), 161–165 (1994)
46. A. Kowal, S.N. Port, R.J. Nichols, Nickel hydroxide electrocatalysts for alcohol oxidation reactions: an evaluation by infrared spectroscopy and electrochemical methods. Catal. Today **38**(4), 483–492 (1997)
47. P.M. Robertson, On the oxidation of alcohols and amines at nickel oxide electrodes: mechanistic aspects. J. Electroanal. Chem. Interfacial Electrochem. **111**(1), 97–104 (1980)
48. A. Cuña, C. Reyes Plascencia, E.L. da Silva, J. Marcuzzo, S. Khan, N. Tancredi, M.R. Baldan, C. de Fraga Malfatti, Electrochemical and spectroelectrochemical analyses of hydrothermal carbon supported nickel electrocatalyst for ethanol electro-oxidation in alkaline medium. Appl. Catal. B Environ. **202**, 95–103 (2017)
49. X. Cui, W. Guo, M. Zhou, Y. Yang, Y. Li, P. Xiao, Y. Zhang, X. Zhang, Promoting effect of Co in Ni_mCo_n (m+n=4) bimetallic electrocatalysts for methanol oxidation reaction. ACS Appl. Mater. Interfaces **7**(1), 493–503 (2015)
50. N.A.M. Barakat, M.A. Abdelkareem, H.Y. Kim, Ethanol electrooxidation using cadmium-doped cobalt/carbon nanoparticles as novel non precious electrocatalyst. Appl. Catal. A Gen. **455**, 193–198 (2013)
51. D. Friebel, M.W. Louie, M. Bajdich, K.E. Sanwald, Y. Cai, A.M. Wise, M.-J. Cheng, D. Sokaras, T.-C. Weng, R. Alonso-Mori, R.C. Davis, J.R. Bargar, J.K. Nørskov, A. Nilsson, A.T. Bell, Identification of highly active Fe sites in (Ni,Fe)OOH for electrocatalytic water splitting. J. Am. Chem. Soc. **137**(3), 1305–1313 (2015)
52. K. Kakaei, K. Marzang, One – Step synthesis of nitrogen doped reduced graphene oxide with NiCo nanoparticles for ethanol oxidation in alkaline media. J. Colloid Interface Sci. **462**, 148–153 (2016)
53. Z. Wang, Y. Du, F. Zhang, Z. Zheng, Y. Zhang, C. Wang, High electrocatalytic activity of non-noble Ni-Co/graphene catalyst for direct ethanol fuel cells. J. Solid State Electrochem. **17**(1), 99–107 (2013)
54. G. Karim-Nezhad, S. Pashazadeh, A. Pashazadeh, Electrocatalytic oxidation of methanol and ethanol by carbon ceramic electrode modified with Ni/Al LDH nanoparticles. Chin. J. Catal. **33**(11-12), 1809–1816 (2012)
55. M. Fleischmann, K. Korinek, and D. Pletcher, The kinetics and mechanism of the oxidation of amines and alcohols at oxide-covered nickel, silver, copper, and cobalt electrodes. J. Chem. Soc. Perkin Trans. **2**, 1396-1403 (1972)
56. R. Jiang, D.T. Tran, J.P. McClure, D. Chu, A class of (Pd–Ni–P) electrocatalysts for the ethanol oxidation reaction in alkaline media. ACS Catal. **4**(8), 2577–2586 (2014)
57. X. Lv, Z. Xu, Z. Yan, X. Li, Bimetallic nickel–iron-supported Pd electrocatalyst for ethanol electrooxidation in alkaline solution. Electrocatalysis **2**(2), 82–88 (2011)
58. J.A. Haber, C. Xiang, D. Guevarra, S. Jung, J. Jin, J.M. Gregoire, High-throughput mapping of the electrochemical properties of (Ni-Fe-Co-Ce)Ox oxygen-evolution catalysts. ChemElectroChem **1**(3), 524–528 (2014)
59. L.J. Enman, M.S. Burke, A.S. Batchellor, S.W. Boettcher, Effects of intentionally incorporated metal cations on the oxygen evolution electrocatalytic activity of nickel (oxy)hydroxide in alkaline media. ACS Catal. **6**(4), 2416–2423 (2016)
60. J. Zaffran, M.B. Stevens, C.D.M. Trang, M. Nagli, M. Shehadeh, S.W. Boettcher, M. Caspary Toroker, Influence of electrolyte cations on Ni(Fe)OOH catalyzed oxygen evolution reaction. Chem. Mater. **29**(11), 4761–4767 (2017)
61. T.N. Ramesh, P.V. Kamath, The effect of cobalt on the electrochemical performance of β-nickel hydroxide electrodes. Electrochim. Acta **53**(28), 8324–8331 (2008)
62. J. Li, A. Oudriss, A. Metsue, J. Bouhattate, X. Feaugas, Anisotropy of hydrogen diffusion in nickel single crystals: the effects of self-stress and hydrogen concentration on diffusion. Sci. Rep. **7**(45041) (2017)
63. M. Wehrens-Dijksma, P.H.L. Notten, Electrochemical quartz microbalance characterization of $Ni(OH)_2$-based thin film electrodes. Electrochim. Acta **51**(18), 3609–3621 (2006)